

Fröhlich electron-phonon vertex from first principles

Carla Verdi and Feliciano Giustino*

Department of Materials, University of Oxford, Parks Road, Oxford OX1 3PH, United Kingdom

We develop a method for calculating the electron-phonon vertex in polar semiconductors and insulators from first principles. The present formalism generalizes the Fröhlich vertex to the case of anisotropic materials and multiple phonon branches, and can be used either as a post-processing correction to standard electron-phonon calculations, or in conjunction with *ab initio* interpolation based on maximally localized Wannier functions. We demonstrate this formalism by investigating the electron-phonon interactions in anatase TiO₂, and show that the polar vertex significantly reduces the electron lifetimes and enhances the anisotropy of the coupling. The present work enables *ab initio* calculations of carrier mobilities, lifetimes, mass enhancement, and pairing in polar materials.

PACS numbers: 71.38.-k, 63.20.dk

The electron-phonon interaction (EPI) is a cornerstone of condensed matter physics, and plays important roles in a diverse array of phenomena. Recent years have witnessed a surge of interest in *ab initio* calculations of EPIs, leading to new techniques and many innovative applications in the case of metals and non-polar semiconductors [1–12]. In contrast to this fast-paced progress, in the case of polar semiconductors and insulators the study of EPIs from first principles has not gone very far, owing to the prohibitive computational costs of EPI calculations for polar materials. For example, a fully *ab initio* calculation of the carrier mobility of a polar semiconductor has not been performed yet, while such calculations have recently been reported for non-polar semiconductors such as silicon [13] and graphene [14]. Given the fast-growing technological importance of polar semiconductors, from light-emitting devices to transparent electronics, solar cells and photocatalysts [15–17], developing accurate and efficient computational methods for studying EPIs in these systems is of primary importance.

At variance with metals and non-polar semiconductors, in polar materials two or more atoms in the unit cell carry nonzero Born effective charge tensors [18]. As a consequence, the fluctuations of the ionic positions corresponding to longitudinal optical (LO) phonons at long wavelength generate macroscopic electric fields which can couple strongly to electrons and holes, leading to the so-called Fröhlich interaction [19]. Up to now this interaction has not been taken into account in *ab initio* calculations of EPIs; the two key obstacles towards a description of Fröhlich coupling from first principles are (i) the Fröhlich coupling was designed to describe simple isotropic systems with one LO phonon, and (ii) the electron-phonon vertex diverges for $\mathbf{q} \rightarrow 0$, where \mathbf{q} is the phonon wavevector. The first obstacle relates to the fundamental question on how to define the Fröhlich coupling in the most general way. The second obstacle renders first-principles calculations extremely demanding, since a correct description of the singularity requires a very fine sampling of the Brillouin zone.

In this work we address the challenges (i) and (ii) above by developing a general formalism for first-principles calculations of the Fröhlich vertex. Our strategy consists in separating the short-range and the long-range contributions to the electron-phonon matrix elements, and identifying the Fröhlich coupling with the long-range component. We translate our formalism into a powerful computational scheme, whereby the short-range component is calculated using state-of-the-art Wannier-Fourier electron-phonon interpolation [20], and the singular coupling is calculated using the Born effective charges and the high-frequency dielectric permittivity tensor. As a first demonstration of this approach we calculate carrier lifetimes in anatase TiO₂.

The Fröhlich model [19] describes the interaction of an electron in a parabolic band with a dispersionless LO phonon of frequency ω_{LO} . The electron is in an isotropic dielectric medium with static and high-frequency permittivities ϵ_0 and ϵ_∞ , respectively. In this model the electron-phonon coupling matrix element takes the form:

$$g_{\mathbf{q}} = \frac{i}{|\mathbf{q}|} \left[\frac{e^2}{4\pi\epsilon_0} \frac{4\pi}{N\Omega} \frac{\hbar\omega_{\text{LO}}}{2} \left(\frac{1}{\epsilon_\infty} - \frac{1}{\epsilon_0} \right) \right]^{\frac{1}{2}}, \quad (1)$$

where \mathbf{q} is the phonon wavevector, Ω the unit cell volume, N the number of unit cells in the Born-von Kármán supercell, and e , ϵ_0 , and \hbar are the electron charge, vacuum permittivity, and reduced Planck constant, respectively. Equation (1) shows that the Fröhlich coupling $g_{\mathbf{q}}$ diverges at long wavelengths, $\mathbf{q} \rightarrow 0$. This singularity poses a challenge to *ab initio* calculations of EPIs in polar materials.

In general the vertex describing electron-one phonon interactions can be expressed via the coupling matrix element $g_{m\nu}(\mathbf{k}, \mathbf{q}) = \langle \psi_{m\mathbf{k}+\mathbf{q}} | \Delta_{\mathbf{q}\nu} V | \psi_{n\mathbf{k}} \rangle$. This quantity has the meaning of probability amplitude for the scattering between the initial electronic state $|\psi_{n\mathbf{k}}\rangle$ and the final state $|\psi_{m\mathbf{k}+\mathbf{q}}\rangle$ via the perturbation $\Delta_{\mathbf{q}\nu} V$ due to a phonon with crystal momentum \mathbf{q} , branch ν and frequency $\omega_{\mathbf{q}\nu}$. The matrix elements $g_{m\nu}(\mathbf{k}, \mathbf{q})$ can be calculated starting from density functional perturbation

theory [21], and have been employed to investigate many properties involving EPIs, for example the electron velocity renormalization [22] and lifetimes [23, 24], phonon softening [3] and lifetimes [25, 26], phonon-assisted absorption [27, 28], critical temperature in conventional superconductors [10, 29, 30], and resistivity [13, 14]. The key ingredient of all these calculations is the evaluation of $g_{m\nu\nu}(\mathbf{k}, \mathbf{q})$ on extremely dense Brillouin zone grids, which is computationally prohibitive. This difficulty has been overcome with the development of an *ab initio* interpolation strategy for the electron-phonon vertex [20, 31] based on maximally-localized Wannier functions [32]. The approach of Ref. 20 relies on the spatial localization of the scattering potential and of the electron wavefunctions when expressed in a real-space Wannier representation.

While the method of Ref. 20 was successfully applied to metals and non-polar semiconductors [1, 6, 12, 14, 23, 28, 33, 34], the same strategy breaks down in the case of polar materials. In fact the singularity in Eq. (1) implies that the scattering potential is long-ranged in real space, hence the Fröhlich vertex is not amenable to Wannier-Fourier interpolation. By the same token less refined linear interpolation strategies are equally inadequate.

In order to deal with the polar singularity we separate the short- (\mathcal{S}) and long-range (\mathcal{L}) contributions to the matrix element:

$$g_{m\nu\nu}(\mathbf{k}, \mathbf{q}) = g_{m\nu\nu}^{\mathcal{S}}(\mathbf{k}, \mathbf{q}) + g_{m\nu\nu}^{\mathcal{L}}(\mathbf{k}, \mathbf{q}). \quad (2)$$

If all contributions leading to the long-wavelength divergence are collected inside $g^{\mathcal{L}}$, then the short-range component will be regular and amenable to Wannier-Fourier interpolation. This strategy is analogous to the calculation of LO-TO splittings in polar materials by separating the analytical and non-analytical parts of the dynamical matrix [35].

We now derive an expression for $g^{\mathcal{L}}$ starting from the following *ansatz*: the macroscopic electric field generated by the nuclei and experienced by the electrons can be obtained by associating an electric point dipole $\mathbf{p} = e \mathbf{Z}^* \cdot \mathbf{u}$ to each atom, where $\mathbf{Z}^* = Z_{\alpha\beta}^*$ is the Born effective

charge tensor and $\mathbf{u} = u_{\alpha}$ is the displacement from equilibrium [here and in the following Greek indices indicate Cartesian coordinates, and we use the notations $(\mathbf{B} \cdot \mathbf{c})_{\alpha} = \sum_{\beta} B_{\alpha\beta} c_{\beta}$, $\mathbf{a} \cdot \mathbf{B} \cdot \mathbf{c} = \sum_{\alpha\beta} a_{\alpha} B_{\alpha\beta} c_{\beta}$]. This notion draws from the very definition of Born charges as the sources of the macroscopic polarization [18]. Our ansatz amounts to following similar steps as in the original work of Fröhlich [19], although we are replacing ionic point charges by Born effective charge tensors. A more formal theory of polar electron-phonon coupling can be developed by starting from a many-body approach [36], and using the analytical properties of the dielectric matrix [37]. Since in polar insulators the atomic oscillations around equilibrium take place over timescales which are much longer than the electronic response time, we can assume following Fröhlich [19] that the electrostatic potential generated by the dipole \mathbf{p} is screened by the high-frequency (electronic) permittivity. This choice corresponds to assuming the adiabatic approximation. In the most general case of anisotropic solid this will be given by the tensor $\epsilon_{\infty} = \epsilon_{\infty, \alpha\beta}$. By solving the anisotropic Poisson's equation with the dipole \mathbf{p} placed at the origin of the reference frame we find:

$$V^{\mathcal{L}}(\mathbf{r}) = i \frac{4\pi}{N\Omega} \frac{e}{4\pi\epsilon_0} \mathbf{p} \cdot \sum_{\mathbf{q}} \sum_{\mathbf{G} \neq -\mathbf{q}} \frac{(\mathbf{q} + \mathbf{G}) e^{i(\mathbf{q} + \mathbf{G}) \cdot \mathbf{r}}}{(\mathbf{q} + \mathbf{G}) \cdot \epsilon^{\infty} \cdot (\mathbf{q} + \mathbf{G})}, \quad (3)$$

where \mathbf{G} indicates a reciprocal lattice vector, and the wavevectors \mathbf{q} belong to a regular grid of N points in the Brillouin zone. This result is derived in the Supplemental Material [38]. Now we consider that one contribution in the form of Eq. (3) arises from each atom κ in the position $\tau_{\kappa\mathbf{R}} = \tau_{\kappa} + \mathbf{R}$, where \mathbf{R} denotes a lattice vector. For a given phonon with wavevector \mathbf{q} belonging to the branch ν the atomic displacement pattern is given by $\Delta\tau_{\kappa\mathbf{R}}^{(\mathbf{q}\nu)} = (\hbar/2NM_{\kappa}\omega_{\mathbf{q}\nu})^{\frac{1}{2}} e^{i\mathbf{q}\cdot\mathbf{R}} \mathbf{e}_{\kappa\nu}(\mathbf{q})$. In this expression $\mathbf{e}_{\kappa\nu}(\mathbf{q})$ represents a vibrational eigenmode normalized within the unit cell. If we make the replacement $\mathbf{p} \rightarrow e\mathbf{Z}_{\kappa}^* \Delta\tau_{\kappa\mathbf{R}}^{(\mathbf{q}\nu)}$ inside Eq. (3), we obtain our main result for the matrix element $g^{\mathcal{L}}$:

$$g_{m\nu\nu}^{\mathcal{L}}(\mathbf{k}, \mathbf{q}) = i \frac{4\pi}{\Omega} \frac{e^2}{4\pi\epsilon_0} \sum_{\kappa} \left(\frac{\hbar}{2NM_{\kappa}\omega_{\mathbf{q}\nu}} \right)^{\frac{1}{2}} \sum_{\mathbf{G} \neq -\mathbf{q}} \frac{(\mathbf{q} + \mathbf{G}) \cdot \mathbf{Z}_{\kappa}^* \cdot \mathbf{e}_{\kappa\nu}(\mathbf{q})}{(\mathbf{q} + \mathbf{G}) \cdot \epsilon^{\infty} \cdot (\mathbf{q} + \mathbf{G})} \langle \psi_{m\mathbf{k}+\mathbf{q}} | e^{i(\mathbf{q} + \mathbf{G}) \cdot \mathbf{r}} | \psi_{n\mathbf{k}} \rangle, \quad (4)$$

where the bracket is to be evaluated within the Born-von Kármán supercell. Details about this derivation are provided in the Supplemental Material [38]. If we consider the more restrictive situation of an isotropic dielectric, we find that Eq. (4) reduces correctly to the Fröhlich vertex in Eq. (1). This result can be obtained by using

the relation between the Born charges and the static and high-frequency permittivities [39], and by invoking the Lyddane-Sachs-Teller relations [40]. Since $g^{\mathcal{L}}$ reduces to the Fröhlich limit under the assumptions used in the original work [19], Eq. (4) represents the generalization of the Fröhlich vertex for *ab initio* calculations. We note that

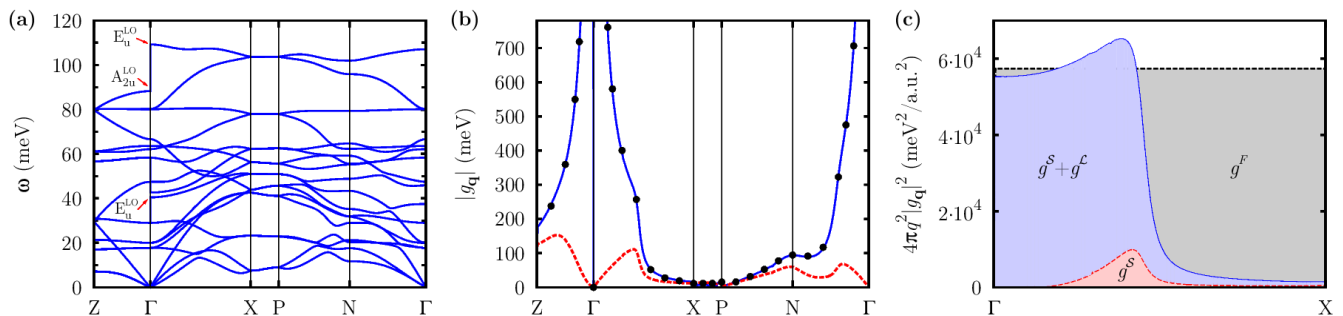


FIG. 1. (a) Calculated phonon dispersions in anatase TiO_2 along high-symmetry lines in the Brillouin zone. The LO phonons discussed in the main text are highlighted by arrows. (b) Calculated electron-phonon matrix elements, with (blue solid lines) and without (red dashed lines) the polar coupling $g^{\mathcal{L}}$ from Eq. (4). The calculations using Wannier-Fourier interpolations (lines) are compared to direct DFPT calculations at each wavevector (filled discs). Here we show the gauge-invariant trace of $|g|^2$ over degenerate states. In the calculation of $g_{m\nu}(\mathbf{k}, \mathbf{q})$ we set the initial electronic state $|\psi_{n\mathbf{k}}\rangle$ to the bottom of the conduction band at Γ , the final electronic state $|\psi_{m\mathbf{k}+\mathbf{q}}\rangle$ to the bottom of the conduction band, and the phonon branch to be the highest (LO) optical mode. (c) Spherical average of the electron-phonon matrix elements, $4\pi q^2 |g|^2$, with (blue) and without (red) the polar coupling, and using the simple Fröhlich model in Eq. (1) (gray).

any choice of the polar electron-phonon coupling which did not have exactly the same limit as Eq. (4) for $\mathbf{q} \rightarrow 0$ would yield a *phonon* self-energy and hence phonon frequencies without the correct LO-TO splitting. In fact, in the long wavelength limit our ansatz leads precisely to the electron-phonon vertex of Ref. 36. The advantage of our formulation is that the physics behind the polar singularity becomes transparent. One interesting property of our polar vertex in Eq. (4) over Eq. (1) is that it naturally takes into account the periodicity of the lattice, which is not the case for the original Fröhlich vertex. Furthermore we do not need to make any assumptions on which LO mode should be considered, since our formalism incorporates seamlessly the coupling to all modes, and the coupling strength is automatically suppressed whenever $\mathbf{Z}_{\kappa}^* \cdot \mathbf{e}_{\kappa\nu}(\mathbf{q})$ is transverse to $\mathbf{q} + \mathbf{G}$.

Taken together Eqs. (2) and (4) provide a practical recipe for calculating EPIs in polar materials. In the simplest approach one could perform calculations involving only the polar coupling $g^{\mathcal{L}}$, in order to determine the magnitude of these effects. In this case the phase factors $\langle \psi_{m\mathbf{k}+\mathbf{q}} | e^{i(\mathbf{q}+\mathbf{G}) \cdot \mathbf{r}} | \psi_{n\mathbf{k}} \rangle$ can safely be replaced by their $\mathbf{q} + \mathbf{G} \rightarrow 0$ limit, δ_{mn} , and the ensuing calculations of $g^{\mathcal{L}}$ become trivial post-processing operations. An example of this calculation is shown in Fig. S2 in the Supplemental Material [38]. A more refined strategy consists of computing the complete matrix elements $g = g^{\mathcal{L}} + g^{\mathcal{S}}$ by exploiting Wannier-Fourier interpolation. In this case we need to perform the following steps: (i) evaluate the complete matrix elements g on coarse Brillouin zone grids; (ii) subtract $g^{\mathcal{L}}$ so as to obtain the short-ranged part of the matrix element, $g^{\mathcal{S}}$; (iii) apply Wannier-Fourier electron-phonon interpolation to the short-range matrix element, following Ref. 20; (iv) add up the short-range part and the long-range part at arbitrary \mathbf{k} and \mathbf{q} points

after interpolation. This strategy enables the calculation of millions of electron-phonon matrix elements for polar materials with *ab initio* accuracy, and at the computational cost of a standard calculation of phonon dispersions. In order to correctly capture the electronic phases we stress that this procedure requires the interpolation of the overlaps in Eq. (4). This is achieved by using the rotation matrices $U_{n\mathbf{k}}$ appearing in the definition of maximally localized Wannier functions [32]: $|w_{m\mathbf{R}}\rangle = \sum_{n\mathbf{k}} e^{-i\mathbf{k} \cdot \mathbf{R}} U_{n\mathbf{k}} |\psi_{n\mathbf{k}}\rangle$. Using this definition and by considering small $\mathbf{q} + \mathbf{G}$ we obtain the result:

$$\langle \psi_{m\mathbf{k}+\mathbf{q}} | e^{i(\mathbf{q}+\mathbf{G}) \cdot \mathbf{r}} | \psi_{n\mathbf{k}} \rangle = \left[U_{\mathbf{k}+\mathbf{q}} U_{\mathbf{k}}^\dagger \right]_{mn}. \quad (5)$$

The matrices $U_{\mathbf{k}}$ are known at every point of the coarse grid from the calculation of maximally localized Wannier functions, and can be obtained at all other points via the interpolation of the electron Hamiltonian [41].

In order to demonstrate our approach we consider the electron-phonon coupling in a prototypical polar semiconductor, anatase TiO_2 . Very recently Fröhlich physics has been studied in this material by means of angle-resolved photoelectron spectroscopy [42]. Figure 1(a) shows the phonon dispersion relations of anatase TiO_2 calculated using **Quantum ESPRESSO** [43] [44]. The polar coupling is manifest in the LO-TO splitting which can be seen around the Γ point for the infrared-active E_u and A_{2u} modes (the LO modes are highlighted by arrows in the plot). In Fig. 1(b) we compare representative electron-phonon matrix elements calculated from DFPT with the result of our polar Wannier-Fourier interpolation, along high-symmetry lines in the Brillouin zone. Our interpolated matrix elements were obtained by performing explicit DFPT calculations on a coarse $4 \times 4 \times 4$ Γ -centered Brillouin zone grid. It is apparent

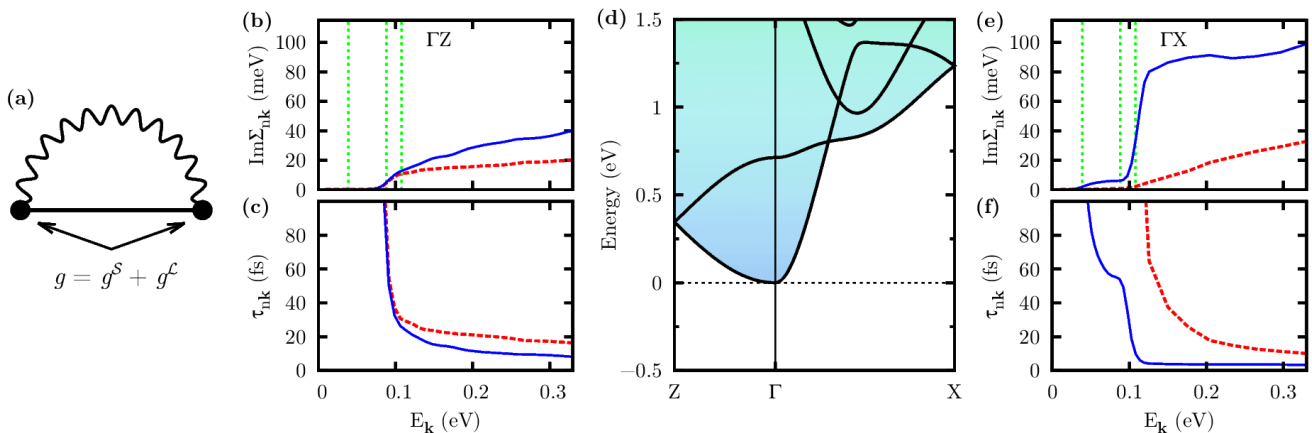


FIG. 2. (a) Diagram of the Migdal self-energy Σ used to calculate electron lifetimes. The straight and wiggly lines represent the electron and phonon Green's functions, respectively. The circles are the electron-phonon matrix elements. (d) Close-up of the conduction bands of anatase TiO_2 near the band bottom at Γ , taken as the zero of the energy. (b), (e) Electron linewidths arising from electron-phonon scattering, $\text{Im}\Sigma$, along the ΓZ and the ΓX lines respectively, near the band bottom. The energies of the LO phonons shown in Fig. 1(a) are indicated by vertical dashed lines. (c), (f) Electron lifetimes from (b) and (e). In (b), (e) and (c), (f) the blue solid lines are computed using the complete vertex, while the red dashed lines are obtained using standard Wannier interpolation [31].

that our method perfectly reproduces the polar singularities at Γ , and the behavior of the matrix element anywhere in the Brillouin zone. For comparison in the same figure we also show the short-range part of the matrix element $|g^S|$ (red line) which is clearly non-singular near Γ . We stress that a standard interpolation strategy *without* taking into account the polar coupling completely fails in reproducing the correct behavior (see Fig. S1 in the Supplemental Material [38]). In order to quantify the importance of the polar divergence, in Fig. 1(c) we consider the quantity $4\pi q^2 |g|^2$ ($q = |\mathbf{q}|$). This quantity is ubiquitous in electron-phonon calculations since most physical properties involve Brillouin zone integrations containing $|g_{mn\nu}(\mathbf{k}, \mathbf{q})|^2 d\mathbf{q}$ [45]. The short-range component (red) severely underestimates the complete coupling strength, even after the singularity has been lifted by the volume element prefactor $4\pi q^2$. Similarly, when using the Fröhlich model in Eq. (1), the coupling is significantly overestimated (gray). This demonstrates that the incorporation of the long-range coupling using Eq. (2) and (4) is essential for *ab initio* calculations of EPIs in polar materials. For completeness Figs. S3 and S4 in the Supplemental Material show that similar conclusions apply to two other prototypical polar compounds, GaN and LiF [38].

As a first example of application of our method we calculate the lifetimes of conduction electrons in anatase TiO_2 arising from the EPI. We determine the lifetimes $\tau_{n\mathbf{k}}$ from the imaginary part of the Migdal electron self-energy $\Sigma_{n\mathbf{k}}$ [Fig. 2(a)], using $\tau_{n\mathbf{k}} = \hbar/2 \text{Im} \Sigma_{n\mathbf{k}}$ [46]. We consider electrons in the conduction band along the ΓZ and the ΓX high-symmetry lines, with energies near the band bottom [Fig. 2(d)]; we evaluate the self-energy using

512,000 inequivalent phonon wavevectors ($80 \times 80 \times 80$ random grid), a broadening of 10 meV, and a temperature of 20 K. The linewidths [Fig. 2(b) and (d)] are negligible below 90 meV: this energy corresponds to the threshold for the emission of the high-frequency A_{2u} LO phonon at Γ . We can also resolve a weaker coupling with a threshold of 40 meV, associated with a E_u LO phonon. Therefore, for electronic states close to the bottom of the conduction band we find that the coupling is dominated by the A_{2u} and E_u LO modes around 100 meV (at 20 K), in agreement with the experimental findings of Ref. [42]. We note that in this case electron-electron interactions do not contribute to the linewidths (within the G_0W_0 approximation) since the electron energy is below the energy thresholds for electron-hole pair generation (the fundamental gap) and for plasmon emission. Turning to the lifetimes, we see in Fig. 2(c) and (f) that these are essentially infinite below the phonon emission threshold, but they are reduced to ~ 3 –9 fs for more energetic electrons. Interestingly the lifetimes are highly anisotropic, varying by a factor of three going from Z to X . This is related to the anisotropy of the band structure, and to the fact that the coupling is strongest for small phonon wavevectors [38]. For comparison we also show in Fig. 2 calculations performed with the standard Wannier interpolation technique [31], which fails to correctly reproduce the matrix elements. The lifetimes are incorrectly enhanced by up to an order of magnitude; at the same time the anisotropy is mostly washed out [red curves in Fig. 2(c) and (f)]. This comparison demonstrates the importance of the polar singularity in the correct calculation of electron lifetimes in TiO_2 . We expect to find similar effects

in related properties, such as polaron binding energy and carrier mobilities.

In conclusion, we introduced a method for studying electron-phonon interactions in polar semiconductors and insulators. Our method generalizes the Fröhlich theory via a consistent description of short-range and long-range contributions to the coupling strength. The present formalism can be employed either for complementing first-principles calculations at no extra cost, or for performing efficient and accurate *ab initio* calculations using Wannier-Fourier interpolation. We expect that our approach will enable the calculation of many properties beyond the reach of current methods, including temperature dependent mobilities in polar semiconductors, dynamics of photoexcited carriers, and superconductivity in doped oxides.

This work was supported by the Leverhulme Trust (Grant RL-2012-001) and the UK Engineering and Physical Sciences Research Council (Grant No. EP/J009857/1). This work used the ARCHER UK National Supercomputing Service via the AMSEC Leadership project, and the Advanced Research Computing facility of the University of Oxford.

Note added. — Recently a related study of polar electron-phonon couplings was reported [47].

* feliciano.giustino@materials.ox.ac.uk

- [1] F. Giustino, M. L. Cohen, and S. G. Louie, *Nature (London)* **452**, 975 (2008).
- [2] G. Profeta, M. Calandra, and F. Mauri, *Nat. Phys.* **8**, 131 (2012).
- [3] S. Pisana, M. Lazzeri, C. Casiraghi, K. S. Novoselov, A. K. Geim, A. C. Ferrari, and F. Mauri, *Nat. Mater.* **6**, 198 (2007).
- [4] C.-H. Park, F. Giustino, M. L. Cohen, and S. G. Louie, *Nano Lett.* **8**, 4229 (2008).
- [5] F. Giustino, J. R. Yates, I. Souza, M. L. Cohen, and S. G. Louie, *Phys. Rev. Lett.* **98**, 047005 (2007).
- [6] F. Giustino, S. G. Louie, and M. L. Cohen, *Phys. Rev. Lett.* **105**, 265501 (2010).
- [7] E. Cannuccia and A. Marini, *Phys. Rev. Lett.* **107**, 255501 (2011).
- [8] G. Antonius, S. Poncé, P. Boulanger, M. Côté, and X. Gonze, *Phys. Rev. Lett.* **112**, 215501 (2014).
- [9] C. E. Patrick and F. Giustino, *Nat. Commun.* **4**, 2006 (2013).
- [10] M. Lüders, M. A. L. Marques, N. N. Lathiotakis, A. Floris, G. Profeta, L. Fast, A. Continenza, S. Massidda, and E. K. U. Gross, *Phys. Rev. B* **72**, 024545 (2005).
- [11] B. Monserrat, N. D. Drummond, C. J. Pickard, and R. J. Needs, *Phys. Rev. Lett.* **112**, 055504 (2014).
- [12] M. Bernardi, D. Vigil-Fowler, J. Lischner, J. B. Neaton, and S. G. Louie, *Phys. Rev. Lett.* **112**, 257402 (2014).
- [13] O. D. Restrepo, K. Varga, and S. T. Pantelides, *Appl. Phys. Lett.* **94**, 212103 (2009).
- [14] C.-H. Park, N. Bonini, T. Sohler, G. Samsonidze, B. Kozinsky, M. Calandra, F. Mauri, and N. Marzari, *Nano Lett.* **14**, 1113 (2014).
- [15] S. Pimpuktar, J. S. Speck, S. P. DenBaars, and S. Nakamura, *Nature Photon.* **3**, 180 (2009).
- [16] M. A. Green, A. Ho-Baillie, and H. Snaith, *Nature Photon.* **8**, 506 (2014).
- [17] A. Fujishima and K. Honda, *Nature (London)* **238**, 37 (1972).
- [18] M. Born and K. Huang, *Dynamical Theory of Crystal Lattices* (Oxford University Press, Oxford, 1954).
- [19] H. Fröhlich, *Adv. Phys.* **3**, 325 (1954).
- [20] F. Giustino, M. L. Cohen, and S. G. Louie, *Phys. Rev. B* **76**, 165108 (2007).
- [21] S. Baroni, S. de Gironcoli, A. Dal Corso, and P. Giannozzi, *Phys. Mod. Phys.* **73**, 515 (2001).
- [22] C.-H. Park, F. Giustino, M. L. Cohen, and S. G. Louie, *Phys. Rev. Lett.* **99**, 086804 (2007).
- [23] C.-H. Park, F. Giustino, C. D. Spataru, M. L. Cohen, and S. G. Louie, *Phys. Rev. Lett.* **102**, 076803 (2009).
- [24] A. Eiguren, S. de Gironcoli, E. V. Chulkov, P. M. Echenique, and E. Tosatti, *Phys. Rev. Lett.* **91**, 166803 (2003).
- [25] B. Liao, B. Qiu, J. Zhou, S. Huberman, K. Esfarjani, and G. Chen, *Phys. Rev. Lett.* **114**, 115901 (2015).
- [26] M. Lazzeri and F. Mauri, *Phys. Rev. Lett.* **97**, 266407 (2006).
- [27] E. Kioupakis, P. Rinke, A. Schleife, F. Bechstedt, and C. G. Van de Walle, *Phys. Rev. B* **81**, 241201 (2010).
- [28] J. Noffsinger, E. Kioupakis, C. G. Van de Walle, S. G. Louie, and M. L. Cohen, *Phys. Rev. Lett.* **108**, 167402 (2012).
- [29] H. J. Choi, D. Roundy, H. Sun, M. L. Cohen, and S. G. Louie, *Nature (London)* **418**, 758 (2002).
- [30] E. R. Margine and F. Giustino, *Phys. Rev. B* **90**, 014518 (2014).
- [31] J. Noffsinger, F. Giustino, B. D. Malone, C.-H. Park, S. G. Louie, and M. L. Cohen, *Comput. Phys. Commun.* **181**, 2140 (2010).
- [32] N. Marzari and D. Vanderbilt, *Phys. Rev. B* **56**, 12847 (1997); I. Souza, N. Marzari, and D. Vanderbilt, *ibid.* **65**, 035109 (2001).
- [33] X.-L. Zhang and W.-M. Liu, *Sci. Rep.* **5**, 8964 (2015).
- [34] N. Vukmirović, C. Bruder, and V. M. Stojanović, *Phys. Rev. Lett.* **109**, 126407 (2012).
- [35] X. Gonze and C. Lee, *Phys. Rev. B* **55**, 10355 (1997).
- [36] P. Vogl, *Phys. Rev. B* **13**, 694 (1976).
- [37] R. M. Pick, M. H. Cohen, and R. M. Martin, *Phys. Rev. B* **1**.
- [38] See Supplemental Material at [url] for details on the derivation of Eq. (3) and Eq. (4), supplemental figure 1, and a discussion of the anisotropic linewidths in Fig. 2.
- [39] O. V. Dolgov and E. G. Maksimov, in *The Dielectric Function of Condensed Systems*, Modern Problems in Condensed Matter Sciences, Vol. 24, edited by L. V. Keldysh, D. A. Kirzhnits, and A. A. Maradudin (Elsevier, Amsterdam, 1989).
- [40] R. H. Lyddane, R. G. Sachs, and E. Teller, *Phys. Rev.* **59**, 673 (1941); W. Cochran and R. A. Cowley, *J. Phys. Chem. Solids* **23**, 447 (1962).
- [41] J. R. Yates, X. Wang, D. Vanderbilt, and I. Souza, *Phys. Rev. B* **75**, 195121 (2007).
- [42] S. Moser, L. Moreschini, J. Jácimović, O. S. Barišić, H. Berger, A. Magrez, Y. J. Chang, K. S. Kim, A. Bostwick, E. Rotenberg, L. Forró, and M. Grioni, *Phys. Rev.*

- Lett. **110**, 196403 (2013).
- [43] P. Giannozzi, S. Baroni, N. Bonini, M. Calandra, R. Car, C. Cavazzoni, D. Ceresoli, G. L. Chiarotti, M. Cococcioni, I. Dabo, A. Dal Corso, S. de Gironcoli, S. Fabris, G. Fratesi, R. Gebauer, U. Gerstmann, C. Gougoussis, A. Kokalj, M. Lazzeri, L. Martin-Samos, N. Marzari, F. Mauri, R. Mazzarello, S. Paolini, A. Pasquarello, L. Paulatto, C. Sbraccia, S. Scandolo, G. Sclauzero, A. P. Seitsonen, A. Smogunov, P. Umari, and R. M. Wentzcovitch, *J. Phys. Condens. Matter* **21**, 395502 (2009).
- [44] We performed ground-state density functional theory calculations using PBE [48] norm-conserving pseudopotentials including the Ti $3s$ and $3p$ semicore states, and a planewaves kinetic energy cutoff of 200 Ry. We sampled the Brillouin zone using a $6 \times 6 \times 6$ Monkhorst-Pack mesh. The phonon dispersions were calculated using density functional perturbation theory (DFPT) [21], by interpolating the frequencies obtained on a $4 \times 4 \times 4$ Brillouin zone grid.
- [45] G. Grimvall, *The Electron-Phonon Interaction in Metals* (North-Holland, New York, 1981).
- [46] G. D. Mahan, *Many-Particle Physics* (Plenum, New York, 1981).
- [47] J. Sjakste, N. Vast, M. Calandra, and F. Mauri, *Phys. Rev. B* **92**, 054307 (2015).
- [48] J. P. Perdew, K. Burke, and M. Ernzerhof, *Phys. Rev. Lett.* **77**, 3865 (1996).

Fröhlich electron-phonon vertex from first principles

Supplemental Material

Carla Verdi and Feliciano Giustino

Department of Materials, University of Oxford, Parks Road, Oxford OX1 3PH, United Kingdom

POINT DIPOLE IN ANISOTROPIC DIELECTRIC MEDIUM

Here we derive Eq. (3) of the main text. Let us consider a point charge Q placed at the position $\boldsymbol{\tau}$. We also include a uniform compensating background $-Q/N\Omega$ so that the supercell is neutral overall (the supercell consists of N unit cells). The medium is an anisotropic dielectric with the permittivity tensor $\boldsymbol{\epsilon} = \epsilon_{\alpha\beta}$. The potential generated by this point charge and the background is obtained as the solution of the Poisson equation [1]:

$$(\nabla \cdot \boldsymbol{\epsilon} \cdot \nabla) \phi(\mathbf{r}; \boldsymbol{\tau}) = -\frac{1}{\epsilon_0} \sum_{\mathbf{T}} \left[Q \delta(\mathbf{r} - \boldsymbol{\tau} - \mathbf{T}) - \frac{Q}{N\Omega} \right], \quad (\text{S1})$$

where \mathbf{T} are the lattice vectors of the Born-von Kármán supercell. The electrostatic potential ϕ is periodic in the supercell, therefore it can be expanded in planewaves as: $\phi(\mathbf{r}; \boldsymbol{\tau}) = \sum_{\mathbf{q}, \mathbf{G}} e^{i(\mathbf{q}+\mathbf{G}) \cdot \mathbf{r}} \phi(\mathbf{q} + \mathbf{G}; \boldsymbol{\tau})$, where the \mathbf{q} vectors belong to a regular grid of N points in the Brillouin zone, and the \mathbf{G} vectors belong to the reciprocal lattice of the crystal unit cell. By replacing this expansion inside Eq. (S1) we obtain, apart from a constant:

$$\phi(\mathbf{r}; \boldsymbol{\tau}) = \frac{4\pi}{\Omega} \frac{Q}{4\pi\epsilon_0} \frac{1}{N} \sum_{\mathbf{q}} \sum_{\mathbf{G} \neq -\mathbf{q}} \frac{e^{i(\mathbf{q}+\mathbf{G}) \cdot (\mathbf{r}-\boldsymbol{\tau})}}{(\mathbf{q} + \mathbf{G}) \cdot \boldsymbol{\epsilon} \cdot (\mathbf{q} + \mathbf{G})}. \quad (\text{S2})$$

Here we made use of the completeness relation: $\sum_{\mathbf{R}} e^{i(\mathbf{q}-\mathbf{q}') \cdot \mathbf{R}} = N\delta_{\mathbf{q}\mathbf{q}'}$, with δ the Kronecker

$$g_{m\nu}^{\mathcal{L}}(\mathbf{k}, \mathbf{q}) = i \frac{4\pi}{\Omega} \frac{e^2}{4\pi\epsilon_0} \sum_{\kappa} \left(\frac{\hbar}{2NM_{\kappa}\omega_{\mathbf{q}\nu}} \right)^{\frac{1}{2}} \sum_{\mathbf{G} \neq -\mathbf{q}} \frac{(\mathbf{q} + \mathbf{G}) \cdot \mathbf{Z}_{\kappa}^* \cdot \mathbf{e}_{\kappa\nu}(\mathbf{q})}{(\mathbf{q} + \mathbf{G}) \cdot \boldsymbol{\epsilon} \cdot (\mathbf{q} + \mathbf{G})} \langle \psi_{m\mathbf{k}+\mathbf{q}} | e^{i(\mathbf{q}+\mathbf{G}) \cdot (\mathbf{r}-\boldsymbol{\tau}_{\kappa})} | \psi_{n\mathbf{k}} \rangle. \quad (\text{S5})$$

As usual the bracket is to be evaluated within the Born-von Kármán supercell. Equation (4) in the main text

The electrostatic potential generated by a dipole $\mathbf{p} = Q\mathbf{u}$ centered at the origin of the reference frame is simply given by $\phi_{\text{dip}}(\mathbf{r}) = \lim_{\mathbf{u} \rightarrow 0} \phi(\mathbf{r}; \mathbf{u}) - \phi(\mathbf{r}; 0)$:

$$\phi_{\text{dip}}(\mathbf{r}) = -i \frac{4\pi}{\Omega} \frac{1}{4\pi\epsilon_0} \frac{1}{N} \sum_{\mathbf{q}} \sum_{\mathbf{G} \neq -\mathbf{q}} \mathbf{p} \cdot \frac{(\mathbf{q} + \mathbf{G}) e^{i(\mathbf{q}+\mathbf{G}) \cdot \mathbf{r}}}{(\mathbf{q} + \mathbf{G}) \cdot \boldsymbol{\epsilon} \cdot (\mathbf{q} + \mathbf{G})}, \quad (\text{S3})$$

which is the same as Eq. (3) of the main text after setting $V^{\mathcal{L}} = -e\phi$.

LONG-RANGE COMPONENT OF THE ELECTRON-PHONON MATRIX ELEMENT

Here we comment on the derivation of Eq. (4) in the main text. The perturbation potential entering the matrix element $g^{\mathcal{L}}$ is obtained by replacing the dipole \mathbf{p} in Eq. (S3) with $e\mathbf{Z}_{\kappa}^* \cdot \Delta\boldsymbol{\tau}_{\kappa\mathbf{R}}^{(\mathbf{q}\nu)}$, for each atom κ in the position $\boldsymbol{\tau}_{\kappa\mathbf{R}} = \boldsymbol{\tau}_{\kappa} + \mathbf{R}$. Here \mathbf{R} is a lattice vector within the Born-von Kármán supercell. As stated in the main text the displacement of each atom in the vibrational eigenmode (\mathbf{q}, ν) is given by $\Delta\boldsymbol{\tau}_{\kappa\mathbf{R}}^{(\mathbf{q}\nu)} = (\hbar/2NM_{\kappa}\omega_{\mathbf{q}\nu})^{\frac{1}{2}} e^{i\mathbf{q} \cdot \mathbf{R}} \mathbf{e}_{\kappa\nu}(\mathbf{q})$. By combining these relations with Eq. (S3) we obtain immediately:

$$V_{\mathbf{q}\nu}^{\mathcal{L}}(\mathbf{r}) = i \frac{4\pi}{\Omega} \frac{e^2}{4\pi\epsilon_0} \sum_{\kappa} \left(\frac{\hbar}{2NM_{\kappa}\omega_{\mathbf{q}\nu}} \right)^{\frac{1}{2}} \sum_{\mathbf{G} \neq -\mathbf{q}} \frac{(\mathbf{q} + \mathbf{G}) \cdot \mathbf{Z}_{\kappa}^* \cdot \mathbf{e}_{\kappa\nu}(\mathbf{q}) e^{i(\mathbf{q}+\mathbf{G}) \cdot (\mathbf{r}-\boldsymbol{\tau}_{\kappa})}}{(\mathbf{q} + \mathbf{G}) \cdot \boldsymbol{\epsilon} \cdot (\mathbf{q} + \mathbf{G})}. \quad (\text{S4})$$

symbol. The matrix elements is calculated as $\langle \psi_{m\mathbf{k}+\mathbf{q}} | V_{\mathbf{q}\nu}^{\mathcal{L}}(\mathbf{r}) | \psi_{n\mathbf{k}} \rangle$:

is obtained from this expression by taking the limit $e^{-i(\mathbf{q}+\mathbf{G}) \cdot \boldsymbol{\tau}_{\kappa}} \rightarrow 1$ inside the bracket.

In principle the definition of $g^{\mathcal{L}}$ given in Eq. (S5) could be altered to include only one reciprocal lattice vector in the summation, namely $\tilde{\mathbf{G}}_{\mathbf{q}}$ such that $|\mathbf{q} + \tilde{\mathbf{G}}_{\mathbf{q}}| = \min_{\mathbf{G}} |\mathbf{q} + \mathbf{G}|$. This would correspond to retaining only the residue of the pole in reciprocal space. In practice this choice is not convenient since it leads to a Fröhlich vertex with discontinuous \mathbf{q} -derivatives at the Brillouin zone boundaries. Instead, in order to minimize the number of \mathbf{G} vectors in Eq. (S5) while preserving a smooth (i.e. infinitely differentiable) Fröhlich matrix element, it is sufficient to truncate the sum to the smallest shell of \mathbf{G} vectors which surrounds \mathbf{q} . In those cases where one is interested in \mathbf{q} vectors within the first Brillouin zone, the above choice corresponds to retaining only the handful of reciprocal lattice vectors which define the first zone.

ANISOTROPY OF THE ELECTRON LINEWIDTHS

The electron linewidths are obtained from the imaginary part of the self-energy Σ arising from the electron-phonon coupling, calculated within the Migdal approximation [2]:

$$\Sigma_{n\mathbf{k}} = \sum_{m\nu\mathbf{q}} |g_{mn\nu}(\mathbf{k}, \mathbf{q})|^2 \left[\frac{n_{\mathbf{q}\nu} + f_{m\mathbf{k}+\mathbf{q}}}{\epsilon_{n\mathbf{k}} - \epsilon_{m\mathbf{k}+\mathbf{q}} + \hbar\omega_{\mathbf{q}\nu} - i\eta} + \frac{n_{\mathbf{q}\nu} + 1 - f_{m\mathbf{k}+\mathbf{q}}}{\epsilon_{n\mathbf{k}} - \epsilon_{m\mathbf{k}+\mathbf{q}} - \hbar\omega_{\mathbf{q}\nu} - i\eta} \right]. \quad (\text{S6})$$

Here $f_{m\mathbf{k}+\mathbf{q}}$ and $n_{\mathbf{q}\nu}$ are the Fermi-Dirac and the Bose-Einstein occupation numbers, respectively, $\epsilon_{n\mathbf{k}}$ and $\epsilon_{m\mathbf{k}+\mathbf{q}}$ are electron energies, $\hbar\omega_{\mathbf{q}\nu}$ is the energy of a phonon with wavevector \mathbf{q} and polarization ν , and η is a small broadening (10 meV).

Figures 2(b) and (e) of the main text show the calculated linewidths of conduction electrons in anatase TiO_2 near the band bottom at Γ . These linewidths are highly anisotropic, varying by a factor of three when going from the Z point to X . This feature is related to the anisotropy of the band structure, and to the fact that the coupling is strongest for small phonon wavevectors. In fact, after we take the limit of vanishing temperature in Eq. (S6), the imaginary part of the self-energy yields a factor $\delta(\epsilon_{n\mathbf{k}} - \epsilon_{m\mathbf{k}+\mathbf{q}} - \hbar\omega_{\mathbf{q}\nu})$ that signifies the energy conservation in the scattering process. In the direction ΓX , the large curvature of the band makes it possible to have electronic transitions with small momentum transfer. In the direction ΓZ the small curvature requires electronic transitions with larger momentum transfer in order to conserve energy. As the polar matrix element goes as $1/q$, the different curvatures lead to enhanced linewidths for electrons with momentum along ΓX , as compared to electrons with momentum along ΓZ . This effect is not correctly captured by using a standard Wannier-Fourier interpolation [red lines in Fig. 2(b) and (e) in the main text]. In particular, the linewidths are systematically underestimated in the standard interpolation, and the error is larger for the linewidths along ΓX , as they involve coupling to phonons with small wavevectors.

-
- [1] L. D. Landau and E. M. Lifshits, *Electrodynamics of Continuous Media* (Pergamon, Oxford, 1960).
 - [2] G. Grimvall, *The Electron-Phonon Interaction in Metals* (North-Holland, New York, 1981).
 - [3] F. Giustino, M. L. Cohen, and S. G. Louie, Phys. Rev. B **76**, 165108 (2007).

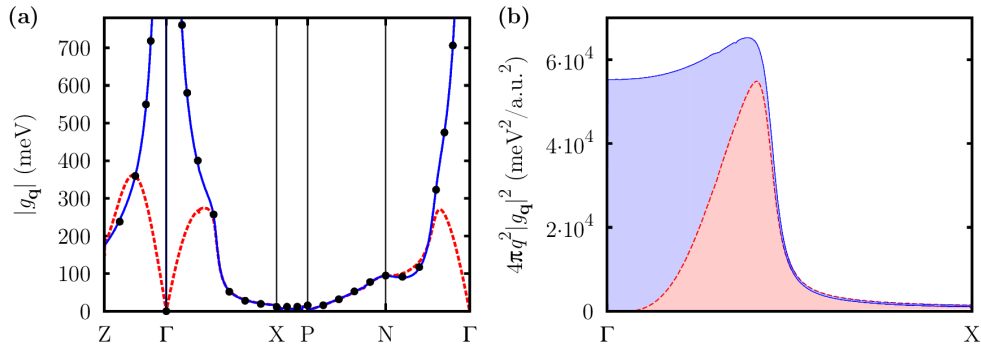


FIG. S1. (a) Calculated electron-phonon matrix elements using our polar Wannier-Fourier interpolation of Eq. (2) in the main text (blue solid lines) and the standard interpolation [3] (red dashed lines). The calculations using Wannier-Fourier interpolations (lines) are compared to direct DFPT calculations at each wavevector (filled discs) as in Fig. 1(b) in the main text. (b) Spherical average of the electron-phonon matrix elements, $4\pi q^2 |g|^2$, with the polar Wannier-Fourier interpolation (blue line) and with the standard interpolation (red line). The standard interpolation corresponds to applying the Wannier-Fourier interpolation technique of Ref. [3] to the entire electron-phonon vertex g on the l.h.s. of Eq. (2). The matrix element g from density-functional perturbation theory goes as $1/|\mathbf{q}|$ for $\mathbf{q} \rightarrow 0$, and vanishes at $\mathbf{q} = 0$ due to the periodic boundary conditions. As a result the Wannier-Fourier method effectively tries to interpolate a strongly fluctuating function, leading to a spurious dip at $\mathbf{q} = 0$ and unphysical behavior elsewhere in the Brillouin zone. This problem is solved by separating the vertex into long- and short-range components, and performing Wannier-Fourier interpolation only on the short-range part g^S .

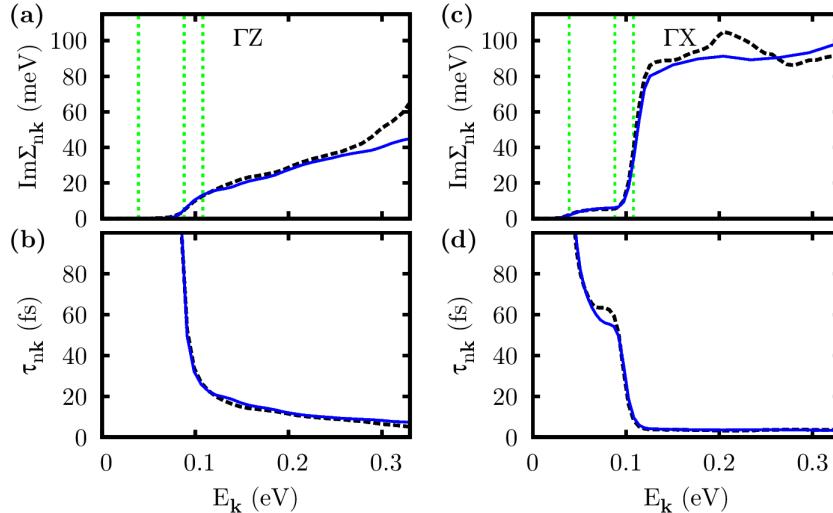


FIG. S2. (a), (c) Electron linewidths in anatase TiO_2 arising from electron-phonon scattering, $\text{Im}\Sigma$, along the ΓZ and the ΓX lines respectively, near the band bottom [as in Fig. 2(b) and (e) of the main text]. The energies of the LO phonons shown in Fig. 1(a) of the main text are indicated by vertical dashed lines. (b), (d) Electron lifetimes from (a) and (c). In (a), (c) and (b), (d) the blue solid lines are computed using the complete electron-phonon vertex g in Eq. (2), while the black dashed lines are obtained by using only the long-range part of the electron-phonon vertex, $g^{\mathcal{L}}$ in Eq. (2). The two approaches yield very similar results in this case. The agreement between calculations performed using g or $g^{\mathcal{L}}$ implies that the electron lifetimes in anatase TiO_2 are dominated by polar interactions with optical phonons.

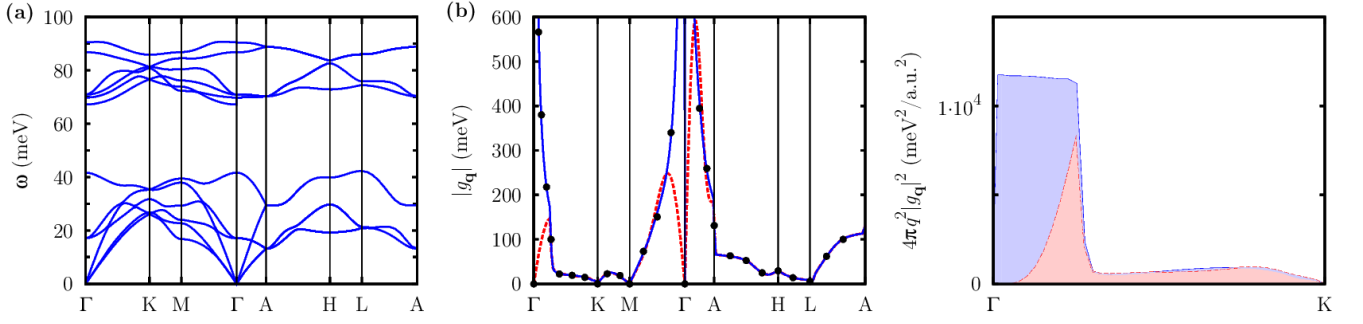


FIG. S3. (a) Calculated phonon dispersions in w-GaN along high-symmetry lines in the Brillouin zone. The phonons are interpolated from a $6 \times 6 \times 6$ Brillouin zone grid. (b) Calculated electron-phonon matrix elements using the present method (blue solid lines) and the standard interpolation [3] (red dashed lines) starting from $6 \times 6 \times 6$ electron and phonon grids. These calculations are compared to direct DFPT calculations at each wavevector (filled discs). Here we show the gauge-invariant trace of $|g|^2$ over degenerate states. In the calculation of $g_{m\nu}(\mathbf{k}, \mathbf{q})$ we set the initial electronic state $|\psi_{m\mathbf{k}}\rangle$ to the top of the valence band at Γ , the final electronic state $|\psi_{m\mathbf{k}+\mathbf{q}}\rangle$ to the top of the valence band, and the phonon branch to be the highest (LO) optical mode. (c) Spherical average of the electron-phonon matrix elements, $4\pi q^2 |g|^2$, with the present method (blue) and with the standard interpolation (red). These calculations were performed using the lattice parameter $a = 3.158 \text{ \AA}$.

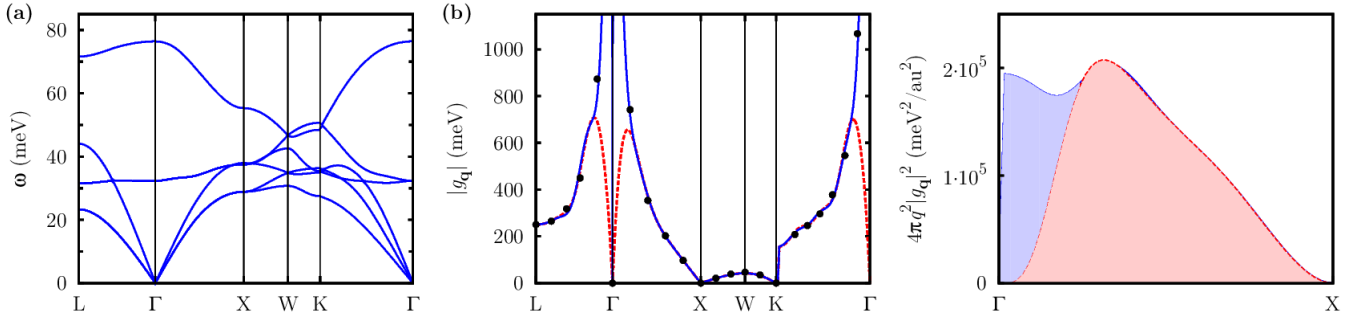


FIG. S4. (a) Calculated phonon dispersions in rocksalt LiF along high-symmetry lines in the Brillouin zone. The phonons are interpolated from a $6 \times 6 \times 6$ Brillouin zone grid. (b) Calculated electron-phonon matrix elements using the present method (blue solid lines) and the standard interpolation [3] (red dashed lines) starting from $8 \times 8 \times 8$ electron and phonon grids. These calculations are compared to direct DFPT calculations at each wavevector (filled discs). As in Fig. S3 we show the gauge-invariant trace of $|g|^2$ over degenerate states, we set the initial electronic state to the top of the valence band at Γ , the final electronic state to the top of the valence band, and the phonon branch to be the highest (LO) optical mode. (c) Spherical average of the electron-phonon matrix elements, $4\pi q^2 |g|^2$, with the present method (blue) and with the standard interpolation (red). These calculations were performed using the lattice parameter $a = 4.026 \text{ \AA}$.